




Article

On the Segmentation of the Cephalonia–Lefkada Transform Fault Zone (Greece) from an InSAR Multi-Mode Dataset of the Lefkada 2015 Sequence

Nikos Svigkas ^{1,2,3,*} , Simone Atzori ², Anastasia Kiratzi ¹ , Cristiano Tolomei ² ,
Andrea Antonioli ², Ioannis Papoutsis ³, Stefano Salvi ² and Charalampos (Haris) Kontoes ³

¹ Department of Geophysics, Faculty of Sciences, Aristotle University of Thessaloniki, 54124 Thessaloniki, Greece

² Osservatorio Nazionale Terremoti, Istituto Nazionale di Geofisica e Vulcanologia, 00143 Roma, Italy

³ Institute of Space Applications and Remote Sensing, National Observatory of Athens, 15236 Athens, Greece

* Correspondence: svigkas@geo.auth.gr

Received: 17 July 2019; Accepted: 6 August 2019; Published: 8 August 2019



Abstract: We use Interferometric Synthetic Aperture Radar (InSAR) to study the Cephalonia–Lefkada Transform Fault Zone (CTF) in the Ionian Sea. The CTF separates continental subduction to the north from oceanic subduction to the south, along the Hellenic Subduction Zone. We exploit a rich multi-modal radar dataset of the most recent major earthquake in the region, the 17 November 2015 Mw 6.4 event, and present new surface displacement results that offer additional constraints on the fault segmentation of the area. Based on this dataset, and by exploiting available information of earthquake relocation, we propose a new rupture process for the 2015 sequence, complementary to those published already. Our modelling includes an additional southern fault segment, oblique to the segment related with the mainshock, which indicates that the CTF structure is more complex than previously believed.

Keywords: InSAR; fault segmentation; Cephalonia–Lefkada Transform Fault; seismology

1. Introduction

The Cephalonia–Lefkada Transform Fault Zone (CTF) in western Greece (Figure 1a), connects two different subducting regimes: subduction of continental lithosphere to the north, with subduction of oceanic lithosphere to the south [1]. The CTF is known for its frequent seismic activity with a well-known historical record [2] and is related to dextral-strike slip motions, which sometimes are connected with thrust components [3–6]. The CTF consists of two active segments: the Cephalonia segment and the Lefkada segment, which run parallel and very close to the western coastline of these islands [4]. The exact mapping of the fault trace is still not known, and its position is inferred, mainly, from the bathymetry.

On 17 November 2015, an earthquake (Mw 6.4) (Figure 1b) struck the western coast of Lefkada island, which stimulated a wealth of publications [7–18]. Sokos et al. [19] were the first to identify that the mainshock broke a strong asperity, left unbroken, in-between two large subevents of the previous 2003 doublet earthquake of Mw 6.2. The same authors, using seismic waveforms, modelled the 2015 event as a multiple point source event, with two well-resolved sources close to Lefkada and a third southern one, less reliable, located at the latitude of the tip of Cephalonia island, offshore. It is noteworthy that the recent (in 2003, 2014, and 2015) events that ruptured parts of the CTF, were all modelled as multiple source events, which indicates faulting complexity [13,19,20]. Papadimitriou et al. [21], using high precision aftershocks of the 2015 sequence, proposed that the area has a network of fault segments, which in some cases are not clearly identified or easily distinguished.

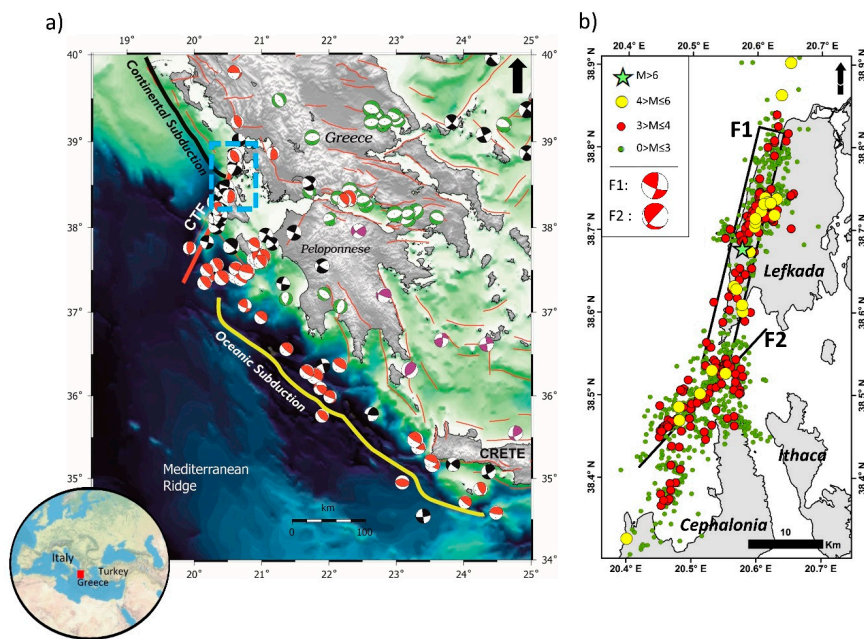


Figure 1. (a) Tectonic setting in the western Hellenic Subduction Zone, depicting the two different subduction regimes, which are offset (~100 km) by the operation of the Cephalonia Transform Fault Zone (CTF). Beach balls denote focal mechanisms of $M > 5.5$ earthquakes, and the magenta colors denote focal depths > 50 km. Black beach balls = strike-slip faulting, red = thrust/reverse faulting, and green = normal faulting. The dashed blue rectangle indicates the area of this study. The red rectangle in the lower left inset globe map is the locus of interest. (b) Map showing the Lefkada 2015 relocated seismic sequence (location data are from [21]) and our proposed fault segmentation (F1 and F2) for the Cephalonia–Lefkada Transform Fault zone.

This complexity is also reflected in the modelling of geodetic data. For example, Ganas et al. [10], based on InSAR and Global Positioning System (GPS) data, presented two uniform slip fault models; one with a unique fault and another one with two faults. Their preferred solution is the two-fault uniform slip model, which comprises of the main fault alongside a smaller fault, parallel to the main one, located partly onshore the island of Lefkada, close to the latitude of the mainshock. Bie et al. [8] used Sentinel-1 imagery as input and performed a series of tests to identify the slip distribution. They show three slip patches in their preferred slip distribution. The southern patch is related with the displacement detected at the tip of Cephalonia island, and according to the authors this southern slip patch was constrained only by their Sentinel descending data. Moreover, this slip patch was defined to be at depths > 10 km, and [8] claim that it was not well resolved by their dataset. It must be noted, though, that monitoring tectonic phenomena in the Ionian Sea is a challenging task, and to elucidate the fault segmentation is difficult due to the sparse distribution of the seismographic and geodetic data, as previously mentioned also by [8,9,12,19].

The advent of remote sensing and, more specifically, the radar satellite data have provided new means of research to the scientific community for earthquake studies [22–27]. The aim of this study is to examine the fault segmentation of the CTF, taking advantage of new remote sensing radar data. The new radar datasets used here (Radarsat-2 and ALOS-2) have not been previously exploited, and they consist of imagery from different viewing geometries. These are utilized together with Sentinel-1 data and provide a clearer picture regarding the displacement that occurred on both the Lefkada and the Cephalonia islands.

The deformation induced by the 2015 earthquake sequence, detected by this new multi-sensor InSAR dataset, together with the exploitation of external data (relocated aftershocks), lead to a more complex fault setting, and to new insights in terms of the fault segmentation and the tectonic processes currently acting at the CTF.

2. Data and Methods

SAR interferometry was used here to calculate displacement of the earth's surface caused by the Lefkada earthquake, based on a diverse dataset consisting of multi-band (C-, X-, and L-) multi-resolution SAR imagery. Initially we considered 4 Sentinel-1 C-band (European Space Agency) images, 2 from ascending and 2 from descending orbits, 4 Radarsat C-band (Canadian Space Agency) images from ascending orbits, 2 ALOS L-band (Japanese Aerospace Exploration Agency,) wide-swath images from descending orbits, and 8 ascending COSMO-SkyMed X-band images (Italian Space Agency). After calculating several differential interferograms, a number of them was discarded due to the excessive impact of low interferometric coherence (e.g., Figure S1). The analysis was therefore carried out with the datasets presented in Table 1.

Table 1. Radar data used.

Satellite	Master Date (m/d/y)	Slave Date (m/d/y)	Temporal Baseline (days)	Normal Baseline (m)	Pass	Linear Inversion RMS (m)
Radarsat-2	2/21/2014	12/1/2015	648	165.4	Ascending	0.016
Sentinel-1	11/5/2015	11/17/2015	12	22.5	Ascending	0.018
ALOS-2	10/12/2015	11/23/2015	42	77.35	Descending	0.025
Sentinel-1	11/11/2015	11/23/2015	12	66.2	Descending	0.012

InSAR processing was carried out with the “repeat-pass” approach [28] using the SARscape software. After coregistering the pre-event and the post-event images, the phase difference was calculated and the topographic phase contribution removal was achieved using the shuttle radar topography mission (SRTM) digital elevation model [29]. Spatially correlated noise was filtered with the approach of Goldstein et al. [30], and the wrapped interferometric phase was then unwrapped with a minimum cost flow algorithm [31]. We then proceeded to the phase (radians) to displacement (meter) conversion and geocoding, and finally we obtained deformation maps in the satellite line-of-sight (LoS) (Figure 2).

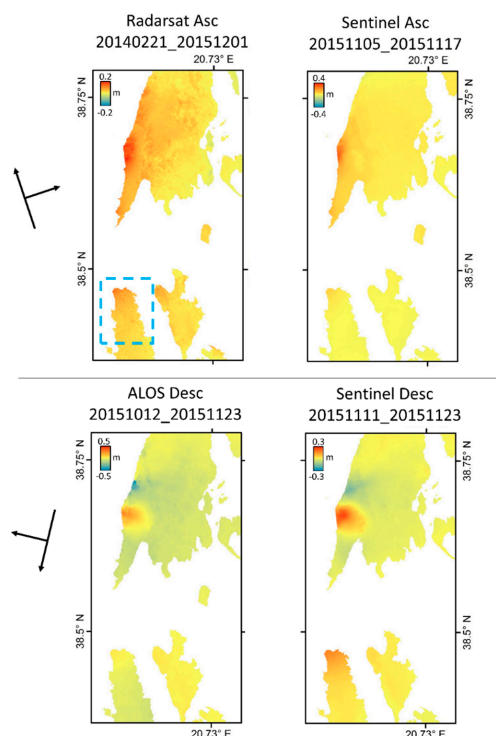


Figure 2. Displacement pattern from the different SAR sensors. The blue dashed rectangle is the area shown in Figure 3.

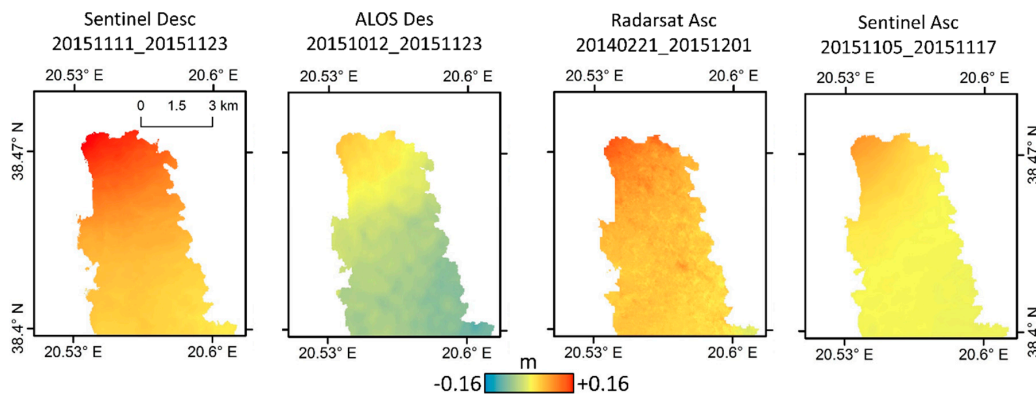


Figure 3. Detail of the unwrapped interferograms used in this study, showing the deformation at the northern tip of Cephalonia (blue dashed rectangle in Figure 2). The displacement at the tip of Cephalonia is apparent in all interferograms and it is this which offers new constraints on the fault segmentation of the area.

To avoid excessive and unnecessary computational load, all displacement maps were downsampled at regular intervals of 200 m in the epicentral area and of 500 m outside it. We identified the seismic sources by means of equations describing the surface displacement induced by a dislocation in an elastic, homogeneous, and isotropic half-space [32]. The source retrieval was carried out in two steps: initially, the fault geometry and mechanism were modelled through a nonlinear optimization scheme based on the Levenberg–Marquardt algorithm [33,34]. The next stage of the modelling followed the retrieval of the fault plane, and included modelling the dislocation distribution, adopting a linear inversion algorithm [35]. In this inversion approach, we extended the size of the retrieved uniform slip fault planes in order to let the slip vanish at the edges, we then subdivided the faults in 1 km × 1 km sized patches. Imposing constraint of a damped and non-negative solution [36], we solved the system:

$$\begin{bmatrix} d \\ 0 \end{bmatrix} = \begin{bmatrix} G \\ \epsilon \nabla^2 \end{bmatrix} \cdot m \quad (1)$$

where d is the InSAR data, G is the Green's functions matrix, ∇^2 is the Laplacian operator, and ϵ is the damping factor obtained by trial-and-error [36]. To adopt a value for the latter, we selected the best compromise between best data fit and fault reliability according to the resulting slip distribution and peak slip values. Finally m is the vector of parameters.

3. Deformation and Seismic Source Modelling Results

The 2015 sequence affected the surface of both Lefkada and Cephalonia islands (Figure 2). The differences in patterns of the displacement results is expected, due to the different viewing angles of the satellites. When looking at all the unwrapped results, the differences between the ascending and the descending acquisitions indicate a horizontal movement (Figure 2). The Sentinel and Radarsat ascending interferograms indicate that both islands (Lefkada and Cephalonia) approached the satellite sensors. As also stated by Bie et al. [8], the Sentinel descending displacement result is more complicated: looking from north to south, on Lefkada at first there is a small signal of negative displacement and then a lobe of positive displacement. Then at the tip of Cephalonia there is also a displacement signal. The ALOS descending result confirms the pattern of the Sentinel descending and offers additional input on the descending viewing geometry. The two lobes on Lefkada, as seen in the descending unwrapped pairs, are part of the classic strike-slip deformation pattern (the rest is covered by the sea body). Previous studies have noted the existence of displacement at the tip of Cephalonia [7,8,10]. The geodetic InSAR results, presented here (Figure 2), provide additional evidence on the displacement at the northern tip of Cephalonia. This, in turn, offers additional constraints regarding the fault segmentation, as shown in the next section. As can be seen in Figure 3, the northern edge of Cephalonia has a positive

displacement pattern, which is evident in all the InSAR results. The wrapped interferograms, the consideration of potential atmospheric artefacts, alongside the InSAR uncertainties, can be found in the supplement.

3.1. Single Fault Model

Initially, we attempted to jointly model our InSAR results with GPS data [9,10,12]. However, the joint geodetic inversion led to large residuals in both datasets. The projection of the three components of GPS measurements into the LoS of every InSAR dataset confirmed a disagreement between the GPS projected values and the InSAR results. In fact, the GPS and InSAR inconsistency is not surprising and it was already observed [11]. While we cannot exclude potential sources of error, this divergence could be attributed, as also stated by Melgar et al. [11], to early afterslip signal contained in InSAR maps, taking into account that the InSAR data include few days of possible slow deformations after the mainshock [7,8,11]. It is thus possible that our dataset contains postseismic signal; the InSAR input is, of course, still essential since our goal is to define the fault segmentation of the area. Given the unavailability of published GPS measurements capturing the displacement at the northern tip of Cephalonia, we proceeded using only the InSAR results in the inversion. Moreover, InSAR offers spatially well-constrained slip patterns, especially for the shallow earthquake events, and is able to identify complex fault segmentations [37].

We firstly performed the nonlinear inversion to identify the faulting geometry and mechanism, assuming that rupture occurred on a single fault. For setting an initial range of allowed values for the fault parameters, we took into consideration the already published ones for the Lefkada 2015 event. In this inversion, every parameter was left free, except the dip value that could not be constrained, thus we adopted a dip of 70° in accordance with [7]. However, a single fault solution was able to model only the displacement of the Lefkada island. A successful reproduction of the displacement at the northern tip of Cephalonia could not be attained (Figure S5). Therefore, the single fault solution was considered insufficient for modelling our dataset.

3.2. Two-Fault Model

Subsequently, we attempted to model the detected displacement using a two-fault model, by adding also a southern fault segment (F2), and we repeated the previous procedure. The deformation signal demanded to lower the number of free parameters. Thus, we kept fixed the parameters of one of the faults, adopting the values previously found with the one-fault solution, which had successfully modelled the displacement of Lefkada. The location and the strike of the second fault segment (F2, Figure 1b) was based on the relocated seismicity of Papadimitriou et al. [21]. Moreover, topographic profiles along part of the F2 segment show that the fault passes by a bathymetric feature that could be related with tectonic activity. More specifically, the fault is located at the peaks of the bathymetric curvature (Figure 4). The dip angle was grid searched in terms of the lowest root-mean-square (RMS) values, which were obtained for dips in the range 80° to 90° , with the lowest values indicating a vertical fault. This is in accordance with Papadimitriou et al. [21], which state that the aftershock locations possibly indicate a vertical structure at that specific area. Results of the nonlinear inversion are summarized in Table S1 and uncertainties are shown in Figures S6 and S7. The RMS values are included in Table S2.

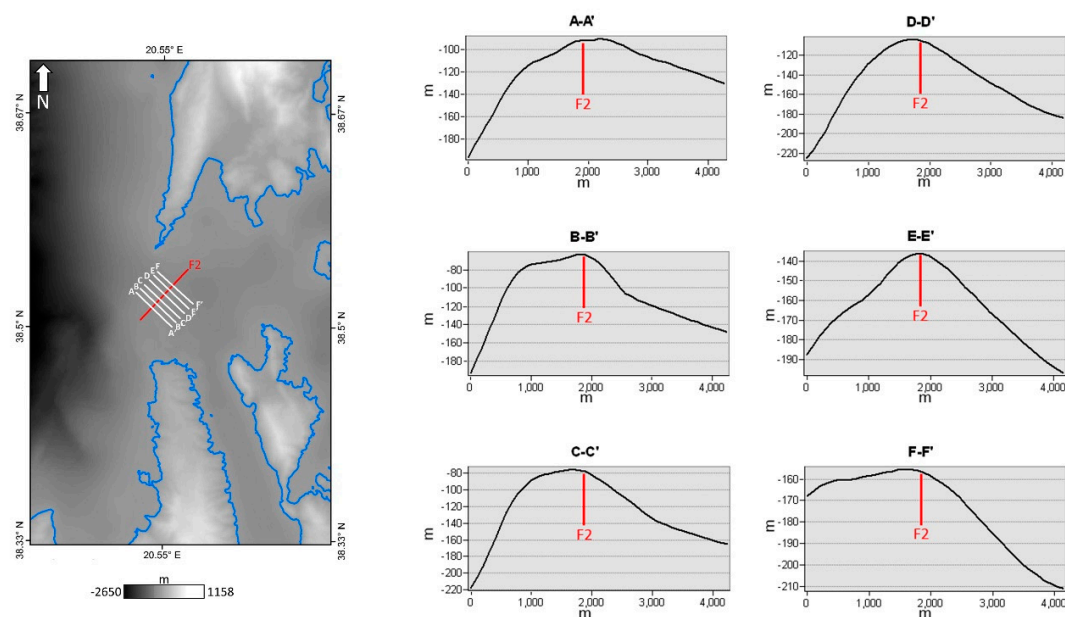


Figure 4. Topography [38] of the study area. A profile screening along the segment F2 indicates the existence of a seafloor feature. The red line is the southern fault segment F2. The white lines A-A', B-B', C-C', D-D', E-E', and F-F' are the bathymetric profiles. In each profile graph, the location of F2 along the profile is noted with a red line.

After defining a geometry assuming a uniform slip, we estimated the slip distribution on the two fault planes. It can be seen in Figure 5a,b that the northern fault segment (F1), which projects underneath the Lefkada island, hosted three separated slip patches. The middle patch, which was the one located at the locus of the mainshock (green asterisk in Figure 5a), had a length of about 8 km and a width of 6 km; the peak slip is 2.9 m and this was the highest slip value overall. The southernmost slip patch of F1 expressed a peak slip of 1.7 m. The northern part of F1 hosted a smaller-sized slip patch with peak slip of 0.6 m that did not reach the surface. The locus of the major slip patch and its peak values at shallow depths can explain the damage pattern (rockfalls, landslide phenomena, building failures) observed in-situ [10,14–17,39]. The main amount of slip on F1 is expressed above 7 km and there is no slip below 10 km. The southern fault segment (F2), hosted a single slip patch with a peak slip of 1.6 m that did reach the seafloor surface. This is the slip patch that predicts the deformation signal of northern Cephalonia (Figure 3). Results indicate that on F2 there was no on-fault dislocation below 6 km.

The root-mean-square (RMS) values of linear inversion for each SAR dataset are shown in Table 1, the source results of this study are in Table 2, while the fits to the data are included in the central and right panels of Figure 6. To evaluate the resolution power of the data, we also performed the source modelling using the variable patch size “full resolution” method introduced by Atzori and Antonioli [40] (Supporting Information). The variable patch size slip pattern is in accordance with the slip distribution presented here, validating our preferred solution.

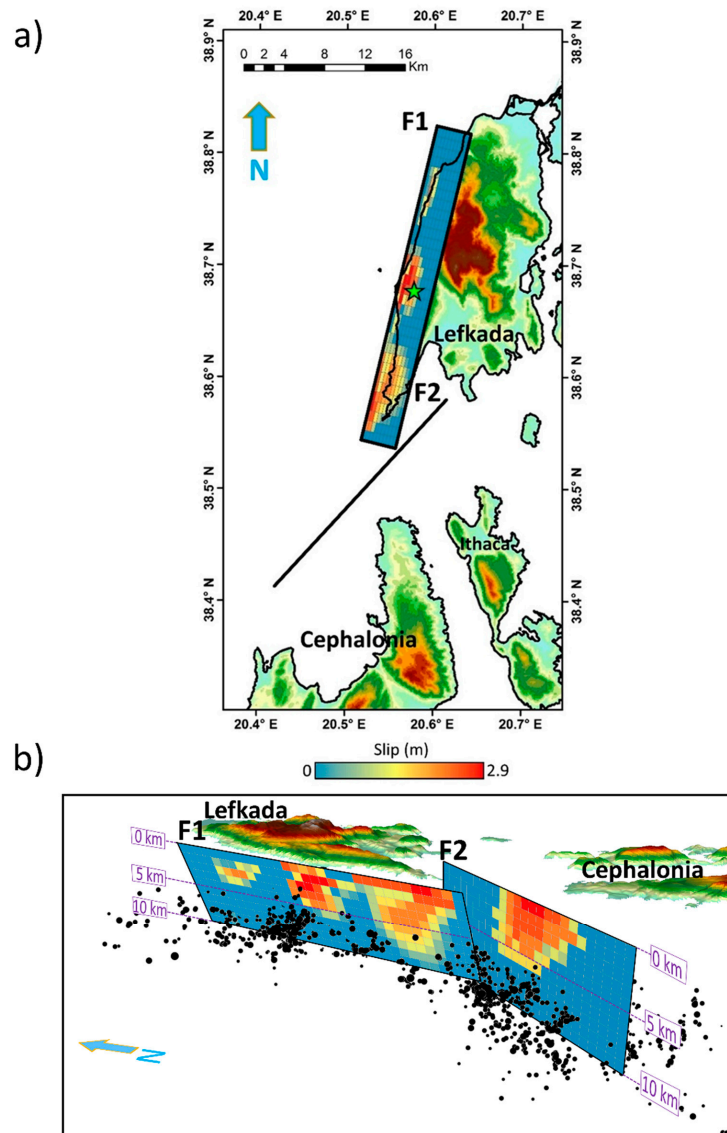


Figure 5. Map showing the two fault segments and the slip distribution. (a) Plane view (green asterisk denotes the mainschock). (b) Three-dimensional (3D) view.

Table 2. Source parameters of the two-fault segments.

Segment F1					
Strike°	Dip°	Rake°	Length (km)	Width (km)	Max Slip (m)
13	70	158	32	10	2.9
Segment F2					
Strike°	Dip°	Rake°	Length (km)	Width (km)	Max Slip (m)
43	90	108	25	10	1.6

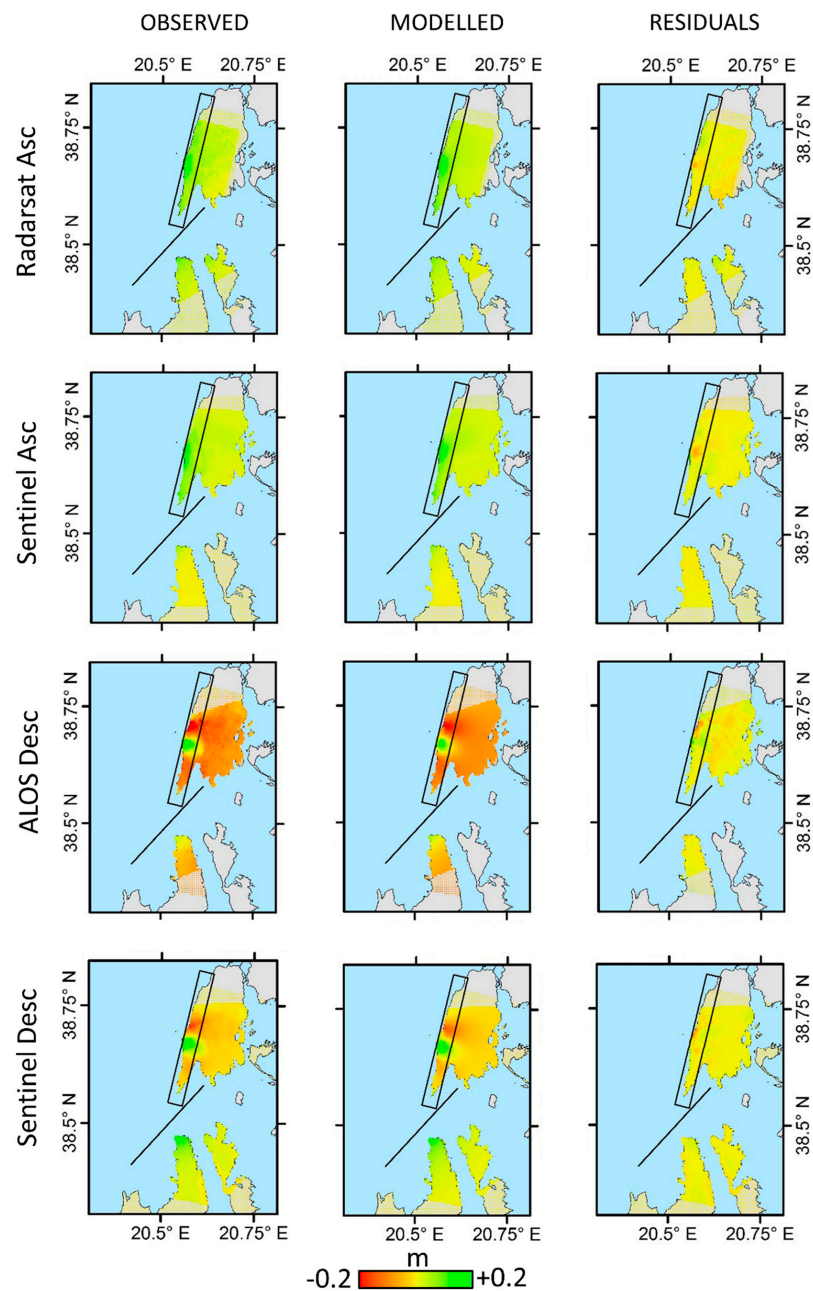


Figure 6. Observed, modelled, and residuals of the linear inversion.

Since we present here a new fault segmentation (2 segments, striking obliquely to each other), a straight comparison of our slip distribution with previous studies is not feasible. Our F1 segment is the only one that could be compared to other slip models, at a first approximation, as published slip distributions are only provided for a single fault segment. Our estimated peak slip of 2.9 m is comparable to the 2.3 m calculated by Chousianitis et al. [9]. Additionally, our model predicts a small slip pattern to the northeast of the Lefkada island. This patch, with slightly different characteristics, also appears in the models of Avallone et al. [7] and Chousianitis et al. [9].

4. Further Interpretation of the Two-Fault Model

Stress Transfer Loading

We used the obtained source mechanisms (Table 2) to investigate a potential stress interaction between F1 and F2 (with F2 as receiver fault). A similar scenario was previously examined [21],

with a different fault configuration for the receiver fault, than the one we adopt. Here, based on our slip distributions, the static Coulomb stress changes ΔCFF , taking into account the pore pressure contribution, were estimated as [41]:

$$\Delta CFF = \Delta\tau + \mu' \Delta\sigma_n \quad (2)$$

where $\Delta\tau$ is the shear stress, $\Delta\sigma_n$ is the normal stress change (unclamping is positive), and μ' is the apparent friction coefficient where $\mu' = \mu (1 - B)$ and B is the Skempton coefficient. Here, μ' was adopted to be 0.4 [42]. Positive ΔCFF indicates that failure is promoted. In the opposite case (negative value), failure is suppressed.

Figure 7 summarizes the results, which indicate that the slip distribution of F2 occurred at an area of positive stress loading (max 0.35 MPa) caused by F1.

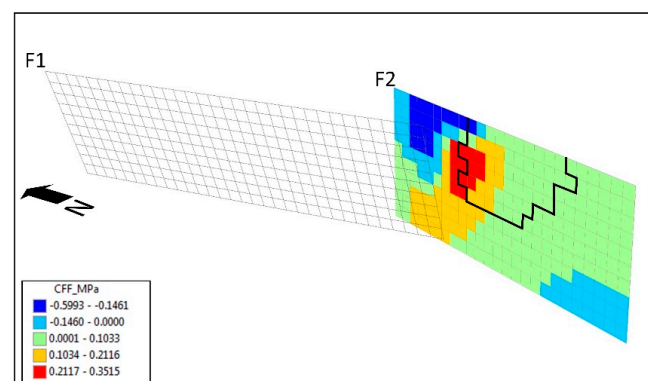


Figure 7. Coulomb stress changes caused from F1 onto the receiver fault F2. The black-noted polygon on F2 denotes the extent of the source's slip distribution.

InSAR cannot offer information on the deformation at the areas that are covered by water bodies. The same limitation exists for the few on-land GPS stations that are installed at the area. Based on all the previous results of this study, we present in the supplementary material the reconstruction of the three dimensional displacement that took place during the 2015 Lefkada sequence and how it evolved.

5. Discussion and Conclusions

We exploited new InSAR multi-modal data from different satellites and orbit modes to revisit the displacement pattern of the Lefkada and Cephalonia islands (Ionian Sea) caused by the occurrence of the 2015 Lefkada earthquake sequence. The displacement fields retrieved here support the operation of a more complex set of structures for the 2015 case study. The InSAR input indicates that a rupture of a single fault, parallel to the western coastline of Lefkada island, is not able to account for the entire observed displacement pattern. It is the observed displacement at the northern tip of the Cephalonia island, which requires a second fault segment, to be sufficiently modelled.

We agree with Ganas et al. [10] about the general concept of a second fault segment, and we also agree with Bie et al. [8] about the fact that the signal at the tip of Cephalonia is an important feature to be considered in the modelling procedure. The importance of the signal at the tip of Cephalonia was furtherly highlighted in our study, and additional information on it was obtained by the specific InSAR dataset used. Our radar signal provided more insights on the on-land deformation pattern of both islands, and as a consequence, it offered better constraints regarding the fault segmentation. We further investigated the multi-segment hypothesis, and building upon the study of Papadimitriou et al. [21] we were able to present a new fault segmentation that predicts well all the InSAR displacement data (both ascending and descending), which is at the same time justified by the relocated seismicity, the seafloor bathymetry, and the stress transfer computation.

Our preferred model identifies two distinct fault segments, which are both required to successfully interpret the geodetic data: a northern fault, bordering the western coastline of Lefkada, associated with the mainshock, encompassing three discrete slip patches, and a secondary southern fault segment, oblique to the northern segment, hosting a single slip patch, at a shallow depth. For this southern segment, no slip is evident below 6 km. The detected dip-slip of the movement of F2 is unfavourably oriented, being a pseudo-vertical fault, not encouraging a dip-slip mechanism; we propose here a possible explanation involving block rotation bounded with pre-existing structure, shown in Figure 8. Regardless of the real block length, by assuming L equal to 1 km, a dislocation of 1.6 m at the surface can be obtained with a negligible rotation α of 0.09° . This movement could have been further facilitated by the existence of evaporites at the broader area [43–47] that can promote frictional instabilities under specific conditions [48].

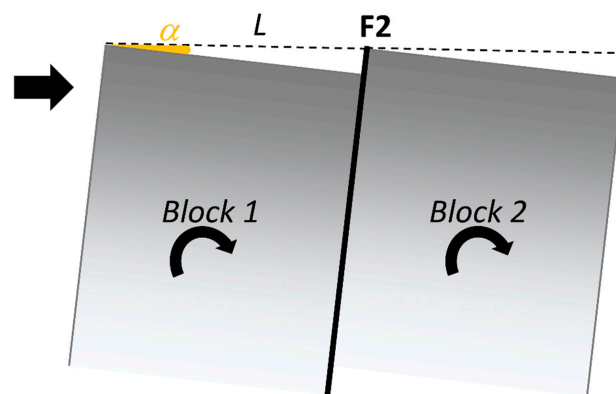


Figure 8. Schematic interpretation of the movement of F2.

To summarize, the Cephalonia–Lefkada Transform Fault (CTF) zone is better viewed as a wide zone where the deformation is taken up by multiple strike-slip fault segments (Figure 9), whereas the thrust components are not negligible at all, possibly related to the Ionian Thrust zone. Here, we proposed the existence of an oblique fault segment (F2) in the intersection of the Cephalonia branch with the Lefkada branch, and it is probable that other similar structures co-exist in the broader region, as Papadimitriou et al. [21] proposed. This oblique fault to the main CTF zone highlights the importance of pre-existing structures in the rupture processes occurring on the CTF. These could partially explain why the Cephalonia Fault Zone tends to rupture in segments with characteristic doublets. At the same time, we believe that the definition of the fault segmentation in the Ionian Sea is still an open issue and further studies are needed to have a clearer picture on the local tectonics.

As the area of the Ionian islands is very active seismically, in the future, new seismic sequences might reveal more information on the processes that take place. However, monitoring should not be focused only on the cases of the major seismic events such as the 2015 one. A continuous monitoring of microseismicity could provide insights about the potential pre-existing structures. These appear to play an important role in the evolution of the seismic sequences. The study of the specific fault network is crucial since it is a threat to the Ionian Islands, which are densely populated, especially during the summer months.

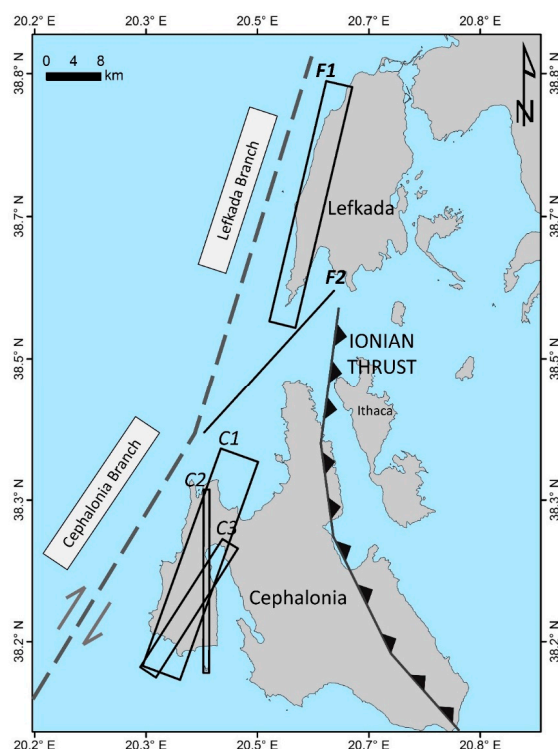


Figure 9. The configuration of the Cephalonia–Lefkada Transform Fault (CTF) zone with the two branches: Cephalonia and Lefkada. The black rectangles outline the faults. F1 and F2 are the sources of the November 2015 earthquake sequence. C1 to C3 are the faults that ruptured during the January–February 2014 earthquakes [20,27]. The CTF is a wide off- and on-shore multi-segmented fault zone; F2 is a structure that separates the CTF into the so-called “Lefkada” and “Cephalonia” branches.

Supplementary Materials: The following are available online at <http://www.mdpi.com/2072-4292/11/16/1848/s1>: Figure S1, an example of a COSMO-SkyMed interferometric result depicting a very low coherence; Figure S2, wrapped interferograms used in the study; Figure S3, comparison of the correlation between InSAR vs GPS (left) and GACOS-corrected InSAR vs GPS (right). Correlation coefficient is the same, indicating that atmospheric artefacts are not covering the tectonic signal; Figure S4, uncertainties of the InSAR analysis; Figure S5, 3D comparison of the observed and modelled (non-linear inversion) interferograms between the 1- and the 2-Fault configurations. (a) 1-Fault configuration is not able to reproduce the displacement at the tip of Cephalonia (green rectangle). (b) 2-Fault configuration reproduces well the displacement in both islands; Figure S6, scattered plots and histograms showing the trade-offs and uncertainties of source parameters of the nonlinear inversion for the northern segment (F1); Figure S7, scattered plots and histograms showing the trade-offs and uncertainties of source parameters of the nonlinear inversion for F2; Figure S8, InSAR slip distribution with a variable patch size. Upper panel, map view; lower panel, 3D view; Figure S9, observed, modelled, and residuals for the variable patch size model of Figure S8; Figure S10, reconstruction in the three dimensions of the evolution of the displacement pattern during the Lefkada 2015 sequence. Phase 1 is the model of the displacement caused by fault F1 (Figure 1b) and Phase 2 is the displacement of the movements caused by both F1 and F2; Table S1, parameters of the nonlinear inversions; Table S2, RMS values of nonlinear inversions.

Author Contributions: Conceptualization, N.S. and S.A.; formal analysis, N.S., S.A., C.T., and A.A.; visualization, N.S., A.K., and S.A.; writing—original draft preparation, N.S.; writing—review and editing, A.K., S.A., A.A., C.T., I.P., S.S., C.K., and N.S.; funding acquisition, S.S., C.K., and A.K. All authors have contributed substantially to this study.

Funding: This work was partially funded by the European Union 7th Framework Program (FP7-REGPOT-2012-2013-1), in the framework of the project BEYOND (Building a Centre of Excellence for EO-based monitoring of Natural Disasters), G. A. 316210. A.K. acknowledges partial support by the project HELPOS (Hellenic System for Lithosphere Monitoring) (MIS 5002697), which is implemented under the action “Reinforcement of the Research and Innovation Infrastructure”, funded by the operational program “Competitiveness, Entrepreneurship and Innovation” (NSRF 2014-2020) and co-financed by Greece and the European Union (European Regional Development Fund).

Acknowledgments: We would like to thank the European Space Agency, the Italian Space Agency, the Canadian Space Agency, and the Japan Aerospace Exploration Agency for the Sentinel, COSMO-SkyMed, Radarsat, and ALOS data, respectively. V. Karakostas and his co-authors are gratefully acknowledged for providing the relocated seismicity. We also thank V. Karakostas for the fruitful discussions. Cristiano Collettini and Antonio Avallone are also thanked for the discussions. Parts of the figures were created with generic mapping tools (GMT) (<http://gmt.soest.hawaii.edu/>).

Conflicts of Interest: The authors declare no conflict of interest.

References

- Pearce, F.D.; Rondenay, S.; Sachpazi, M.; Charalampakis, M.; Royden, L.H. Seismic investigation of the transition from continental to oceanic subduction along the western Hellenic Subduction Zone. *J. Geophys. Res.* **2012**, *117*, B07306. [CrossRef]
- Papazachos, B.C.; Papazachou, C.B. *The Earthquakes of Greece*. 1997. Available online: <http://nemertes.lis.upatras.gr/jspui/handle/10889/817> (accessed on 5 April 2019).
- Kiratzí, A.; Langston, C. Moment tensor inversion of the January 17, 1983 Kefallinia event of Ionian Islands (Greece). *Geoph. Jour. Int.* **1991**, *105*, 529–535. [CrossRef]
- Louvari, E.; Kiratzí, A.; Papazachos, B.C. The Cephalonia Transform Fault and its continuation to western Lefkada Island. *Tectonophysics* **1999**, *308*, 223–236. [CrossRef]
- Sachpazi, M.; Hirn, A.; Clément, C.; Haslinger, F.; Laigle, M.; Kissling, E.; Charvis, P.; Hello, Y.; Lépine, J.C.; Sapin, M.; et al. Western Hellenic subduction and Cephalonia Transform: Local earthquakes and plate transport and strain. *Tectonophysics* **2000**, *319*, 301–331. [CrossRef]
- Scordilis, M.; Karakaisis, F.; Karacostas, G.; Panagiotopoulos, G.; Comninakis, E.; Papazachos, C. Evidence for transform faulting in the Ionian Sea: The Cephalonia Island earthquake sequence of 1983. *PAGEOPH* **1985**, *123*, 388–397. [CrossRef]
- Avallone, A.; Cirella, A.; Cheloni, D.; Tolomei, C.; Theodoulidis, N.; Piatanesi, A.; Briole, P.; Ganas, A. Near-source high-rate GPS, strong motion and InSAR observations to image the 2015 Lefkada (Greece) Earthquake rupture history. *Sci. Rep.* **2017**, *7*, 10358. [CrossRef] [PubMed]
- Bie, L.; González, P.J.; Rietbrock, A. Slip distribution of the 2015 Lefkada earthquake and its implications for fault segmentation. *Geoph. Jour. Int.* **2017**, *210*, 420–427. [CrossRef]
- Chousianitis, K.; Konca, A.O.; Tselentis, G.A.; Papadopoulos, G.A.; Gianniou, M. Slip model of the 17 November 2015 Mw =6.5 Lefkada earthquake from the joint inversion of geodetic and seismic data. *Geophys. Res. Lett.* **2016**, *43*, 7973–7981. [CrossRef]
- Ganas, A.; Elias, P.; Bozionelos, G.; Papathanassiou, G.; Avallone, A.; Papastergios, A.; Valkaniotis, S.; Parcharidis, I.; Briole, P. Coseismic deformation, field observations and seismic fault of the 17 November 2015 M = 6.5, Lefkada Island, Greece earthquake. *Tectonophysics* **2016**, *687*, 210–222. [CrossRef]
- Melgar, D.; Ganas, A.; Geng, J.; Liang, C.; Fielding, E.J.; Kassaras, I. Source characteristics of the 2015 Mw6.5Lefkada, Greece, strike-slip earthquake. *J. Geophys. Res. Solid Earth* **2017**, *122*, 2260–2273.
- Saltogianni, V.; Taymaz, T.; Yolsal-Çevikbilen, S.; Eken, T.; Moschas, F.; Stiros, S. Fault Model for the 2015 Leucas (Aegean Arc) Earthquake: Analysis Based on Seismological and Geodetic Observations. *Bull. Seismol. Soc. Am.* **2017**, *107*. [CrossRef]
- Sokos, E.; Zahradník, J.; Gallovic, F.; Serpetsidaki, A.; Plicka, V.; Kiratzí, A. Asperity break after 12 years: The Mw6.4 2015 Lefkada (Greece) earthquake. *Geophys. Res. Lett.* **2016**, *43*. [CrossRef]
- Papathanassiou, G.; Valkaniotis, S.; Ganas, A.; Grendas, N.; Kollia, E. The November 17th, 2015 Lefkada (Greece) strike-slip earthquake: Field mapping of generated failures and assessment of macroseismic intensity ESI-07. *Eng. Geol.* **2015**, *220*, 13–30. [CrossRef]
- Lekkas, E.; Mavroulis, S.; Carydis, P.; Alexoudi, V. The 17 November 2015 Mw 6.4 Lefkas (Ionian Sea, Western Greece) Earthquake: Impact on Environment and Buildings. *Geotech. Eng.* **2018**, *36*, 2109–2142. [CrossRef]
- Lekkas, E.; Mavroulis, S.; Alexoudi, V. Field observations of the 2015 (November 17, Mw 6.4) Lefkas (Ionian sea, western Greece) earthquake impact on natural environment and building stock of Lefkas island. *Bull. Geol. Soc. Greece* **2016**, *50*, 499–510. [CrossRef]

17. Kassaras, I.; Kazantzidou-Firtinidou, D.; Ganas, A.; Tonna, S.; Pomonis, A.; Karakostas, C.; Papadatou-Giannopoulou, C.; Psarris, D.; Lekkas, E.; Makropoulos, K. On the Lefkas (Ionian Sea) November 17, 2015 Mw = 6.5 Earthquake Macroseismic Effects. *J. Earthq. Eng.* **2018**. [[CrossRef](#)]
18. Ganas, A.; Briole, P.; Melgar, D.; Bozionelos, G.; Valkaniotis, S.; Avallone, A.; Papathanassiou, G.; Mendonidis, E.; Elias, P. Coseismic Deformation and Seismic fault of the 17 November 2015 M=6.5 earthquake, Lefkada island. *Bull. Geol. Soc. Greece* **2016**, *50*, 491–498. [[CrossRef](#)]
19. Sokos, E.; Kiratzi, A.; Gallovič, F.; Zahradník, J.; Serpetsidaki, A.; Plicka, V.; Janský, J.; Kostecký, J.; Tselentis, G.A. Rupture process of the 2014 Cephalonia, Greece, earthquake doublet (Mw6) as inferred from regional and local seismic data. *Tectonophysics* **2015**, *656*, 131–141. [[CrossRef](#)]
20. Kiratzi, A. Mechanisms of Earthquakes in Aegean. In *Encyclopedia of Earthquake Engineering*; Beer, M., Kouglioumtzoglou, I.A., Patelli, E., Siu-Kui, I., Eds.; Springer: Berlin/Heidelberg, Germany, 2014; pp. 1–22.
21. Papadimitriou, E.; Karakostas, V.; Mesimeri, M.; Chouliaras, G.; Kourouklas, C.H. The Mw 6.5 17 November 2015 Lefkada (Greece) Earthquake: Structural Interpretation by Means of the Aftershock Analysis. *Pure Appl. Geophys.* **2017**, *174*, 3869–3888. [[CrossRef](#)]
22. Polcari, M.; Palano, M.; Fernández, J.; Samsonov, S.V.; Stramondo, S.; Zerbini, S. 3D displacement field retrieved by integrating Sentinel-1 InSAR and GPS data: The 2014 South Napa earthquake. *Eur. J. Remote Sens.* **2016**, *49*. [[CrossRef](#)]
23. Polcari, M.; Albano, M.; Atzori, S.; Bignami, C.; Stramondo, S. The Causative Fault of the 2016 Mw 6.1 Petermann Ranges Intraplate Earthquake (Central Australia) Retrieved by C- and L-Band InSAR Data. *Remote Sens.* **2018**, *10*, 1311. [[CrossRef](#)]
24. Barba-Sevilla, M.; Baird, B.W.; Liel, A.B.; Tiampo, K.F. Hazard Implications of the 2016 Mw 5.0 Cushing, OK Earthquake from a Joint Analysis of Damage and InSAR Data. *Remote Sens.* **2018**, *10*, 1715. [[CrossRef](#)]
25. Albano, M.; Polcari, M.; Bignami, C.; Moro, M.; Saroli, M.; Stramondo, S. Did anthropogenic activities trigger the 3 April 2017, Mw 6.5 Botswana earthquake? *Remote Sens.* **2017**, *9*, 1028. [[CrossRef](#)]
26. Vajedian, S.; Motagh, M.; Mousavi, Z.; Motaghi, K.; Fielding, E.J.; Akbari, B.; Wetzell, H.U.; Darabi, A. Coseismic Deformation Field of the Mw 7.3 12 November 2017 Sarpol-e Zahab (Iran) Earthquake: A Decoupling Horizon in the Northern Zagros Mountains Inferred from InSAR Observations. *Remote Sens.* **2018**, *10*, 1589. [[CrossRef](#)]
27. Boncori, J.P.M.; Papoutsis, I.; Pezzo, G.; Tolomei, C.; Atzori, S.; Ganas, A.; Karastathis, V.; Salvi, S.; Kontoes, C.; Antonioli, A. The February 2014 Cephalonia earthquake (Greece): 3D deformation field and source modeling from multiple SAR techniques. *Seism. Res. Lett.* **2015**, *86*, 124–137. [[CrossRef](#)]
28. Massonnet, D.; Feigl, K.L. Satellite radar interferometric map of the coseismic deformation field of the M = 6.1 Eureka Valley, California earthquake of May 17, 1993. *Geophys. Res. Lett.* **1995**, *22*, 1541–1544. [[CrossRef](#)]
29. Farr, T.G.; Kobrick, M. Shuttle radar topography mission produces a wealth of data. *Eos Trans.* **2000**, *81*, 583–585. [[CrossRef](#)]
30. Goldstein, R.; Werner, C. Radar Interferogram filtering for geophysical applications Radar interferogram filtering for geophysical applications. *Geophys. Res. Lett.* **1998**, *25*, 4035–4038. [[CrossRef](#)]
31. Costantini, M. A novel phase unwrapping method based on network programming. *Geosci. Remote Sens.* **1998**, *36*, 813–821. [[CrossRef](#)]
32. Okada, Y. Surface deformation due to shear and tensile faults in a half-space. *Bull. Seism. Soc. Am.* **1985**, *75*, 1135–1154.
33. Levenberg, K. A method for the solution of certain problems in least squares. *Q. Appl. Math.* **1944**, *2*, 164–168. [[CrossRef](#)]
34. Marquardt, D. An Algorithm for Least-Squares Estimation of Nonlinear Parameters. *SIAM J. Appl. Math.* **1963**, *11*, 431–441. [[CrossRef](#)]
35. Atzori, S.; Hunstad, I.; Chini, M.; Salvi, S.; Tolomei, C.; Bignami, C.; Stramondo, S.; Trasatti, E.; Antonioli, A.; Boschi, E. Finite fault inversion of DInSAR coseismic displacement of the 2009 L'Aquila earthquake (central Italy). *Geophys. Res. Lett.* **2009**, *36*, L15305. [[CrossRef](#)]
36. Menke, W. *Geophysical Data Analysis: Discrete Inverse Theory*; Academic Press: San Diego, CA, USA, 1989.
37. Elliott, J.R.; Walters, R.J.; Wright, T.J. The role of space-based observation in understanding and responding to active tectonics and earthquakes. *Nat. Commun.* **2016**, *7*. [[CrossRef](#)] [[PubMed](#)]
38. Topographic Data. Available online: <http://www.emodnet-bathymetry.eu> (accessed on 5 April 2019).

39. Kazantzidou-Firtinidou, D.; Kassaras, I.; Tonna, S.; Ganas, A.; Vintzileou, E.; Chesi, C. The November 2015 Mw6.4 earthquake effects in Lefkas Island. In Proceedings of the 1st International Conference on Natural Hazards Infrastructure, Chania, Greece, 18–21 June 2016.
40. Atzori, S.; Antonioli, A. Optimal fault resolution in geodetic inversion of coseismic data. *Geophys. J. Int.* **2011**, *185*, 529–538. [[CrossRef](#)]
41. Harris, R.; Simpson, R.W. Suppression of large earthquakes by stress shadows: A comparison of Coulomb and rate-and-state failure. *J. Geophys. Res.* **1998**, *103*, 24439–24451. [[CrossRef](#)]
42. Papadimitriou, E.E. Mode of strong earthquake recurrence in central Ionian Islands (Greece). Possible triggering due to Coulomb stress changes generated by the occurrence of previous strong shocks. *Bull. Seism. Soc. Am.* **2002**, *92*, 3293–3308. [[CrossRef](#)]
43. Stiros, S.; Pirazzoli, P.; Labore, J.; Laborel-Deguen, F. The 1953 earthquake in Cephalonia (Western Hellenic Arc): Coastal uplift and halotectonic faulting. *Geophys. J. Int.* **1994**, *117*, 834–849. [[CrossRef](#)]
44. Karakitsios, V.; Rigakis, N. Evolution and Petroleum potential of western Greece. *J. Pet. Geol.* **2007**, *30*, 197–218. [[CrossRef](#)]
45. Saltogianni, V.; Moschas, F.; Stiros, S. The 2014 Cephalonia Earthquakes: Finite Fault Modeling, Fault Segmentation, Shear and Thrusting at the NW Aegean Arc (Greece). *Pure Appl. Geophys.* **2018**, *175*, 4145. [[CrossRef](#)]
46. Brooks, M.; Ferentinos, G. Tectonics and sedimentation in the Gulf of Corinth and the Zakynthos and Kefallinia channels, Western Greece. *Tectonophysics* **1984**, *101*, 25–54. [[CrossRef](#)]
47. Velaj, T.; Davison, I.; Serjani, A.; Alsop, I. Thrust tectonics and the role of evaporites in the Ionian Zone of the Albanides. *AAPG Bull.* **1999**, *83*, 1408–1425.
48. Scuderi, M.M.; Niemeijer, A.R.; Collettini, C.; Marone, C. Frictional properties and slip stability of active faults within carbonate–evaporite sequences: The role of dolomite and anhydrite. *Earth Planet. Sci. Lett.* **2013**. [[CrossRef](#)]



© 2019 by the authors. Licensee MDPI, Basel, Switzerland. This article is an open access article distributed under the terms and conditions of the Creative Commons Attribution (CC BY) license (<http://creativecommons.org/licenses/by/4.0/>).